



1 **Isotopic compositions of atmospheric total gaseous mercury in ten Chinese cities and**
2 **implications for land surface emissions**

3

4 Xuewu Fu^{1,2}, Chen Liu^{1,3}, Hui Zhang^{1,3}, Yue Xu¹, Hui Zhang¹, Jun Li⁴, Xiaopu Lyu⁵, Gan Zhang⁴,
5 Hai Guo⁵, Xun Wang¹, Leiming Zhang⁶, Xinbin Feng^{1,2,3}

6 ¹State Key Laboratory of Environmental Geochemistry, Institute of Geochemistry, Chinese Academy of Sciences,
7 Guiyang, 550081, China

8 ²CAS Center for Excellence in Quaternary Science and Global Change, Xi'an, 710061, China

9 ³University of Chinese Academy of Sciences, Beijing, 100049, China

10 ⁴State Key Laboratory of Organic Geochemistry, Guangzhou Institute of Geochemistry, Chinese Academy of
11 Sciences, Guangzhou, 510640, China

12 ⁵Department of Civil and Environmental Engineering, The Hong Kong Polytechnic University, Hong Kong, China

13 ⁶Air Quality Research Division, Science and Technology Branch, Environment and Climate Change Canada,
14 Toronto, Ontario, Canada

15 Correspondence to: Xuewu Fu, fuxuewu@mail.gyig.ac.cn and Xinbin Feng, fengxinbin@vip.skleg.cn

16



17 **Abstract:**

18 Land surface emissions are an important source of atmospheric total gaseous mercury (TGM),
19 however, its role on the variations of TGM isotopic compositions and concentrations has not been
20 properly evaluated. In this study, TGM isotope compositions, a powerful tracer for sources and
21 transformation of Hg, were measured at ten urban sites and one rural site in China. TGM
22 concentrations were higher in summer than in winter in most cities except in Guiyang and
23 Guangzhou in the low latitudes. The summertime high TGM concentrations were coincided with
24 prevailing low TGM $\delta^{202}\text{Hg}$ and high TGM $\Delta^{199}\text{Hg}$ signatures. These seasonal patterns were in
25 contrast with those typically observed in rural areas in the Northern Hemisphere, suggesting
26 atmospheric oxidation chemistry, vegetation activity as well as residential coal combustion were not
27 likely the dominant mechanisms contributing to the TGM concentration and isotopic composition
28 seasonality in Chinese cities. The amplitudes of seasonal variations in TGM concentrations and
29 $\Delta^{199}\text{Hg}$ (or TGM $\delta^{202}\text{Hg}$) were significantly positively (or negatively) correlated with that of the
30 simulated soil GEM emission flux. These results suggest that the seasonal variations in TGM
31 isotopic compositions and concentrations in the ten Chinese cities were likely controlled by land
32 surface emissions that were observed or reported with highly negative $\delta^{202}\text{Hg}$ signatures.

33

34

35 **1. Introduction**

36 Mercury (Hg) is a toxic heavy metal pollutant of global concerns for ecological and human
37 health. Hg in the atmosphere includes three major forms: gaseous elemental mercury (GEM),
38 gaseous oxidized mercury (GOM), and particulate bound mercury (PBM). According to global Hg
39 models, GEM is the dominant form of total gaseous mercury (TGM = GEM + GOM, 88.8~92.9%)
40 and total Hg (88.8~92.8%) in the troposphere (Selin et al., 2007; Holmes et al., 2010; Horowitz et
41 al., 2017), and the fraction of GEM in total atmospheric Hg is thought to be much higher in the
42 planetary boundary layer (PBL) (e.g., on average >95%) than that in the free troposphere
43 (Swartzendruber et al., 2009; Lyman and Jaffe, 2012; Shah et al., 2016). GEM has a long
44 atmospheric residence time and can transport globally through the atmosphere (Obrist et al., 2018).
45 GEM can be deposited onto earth's surface by dry deposition or atmospheric oxidation followed by
46 wet and dry deposition. Once deposited, it could be transformed to methylmercury and subsequently
47 bio-accumulated in the food web, posing a threat to human health and the environment (Obrist et
48 al., 2018). GEM in the atmosphere can be derived from primary anthropogenic, natural and legacy
49 emissions. Land surface emissions are an important source of atmospheric GEM. Total GEM
50 emissions from global land surfaces, although not well constrained, are estimated to range from 600
51 to 2000 Mg/yr, which are in the similar magnitude as the global primary anthropogenic GEM
52 emissions (Selin et al., 2007; Holmes et al., 2010; Pirrone et al., 2010; Agnan et al., 2016). However,
53 to what extent the land surface emissions can contribute to the variations of GEM at local, regional,
54 and global scales has not been well understood.



55 TGM or GEM concentrations in urban areas are generally elevated as compared to rural areas
56 (Fu et al., 2015; Mao et al., 2016), which could be attributed to strong Hg emissions from primary
57 anthropogenic sources, urban surfaces (soil, pavement, building surface, dominantly referred to as
58 “legacy” emissions), and indoor Hg-containing products (Carpi and Chen, 2001; Feng et al., 2005;
59 Eckley and Branfireun, 2008; Rutter et al., 2009). A previous study in Mexico City, Mexico, based
60 on pollution rose and Concentration Field Analysis (CFA), suggested that highly elevated GEM
61 concentrations (mean = 7.2 ng m⁻³) were dominantly (81%) attributed to anthropogenic sources
62 (Rutter et al., 2009). The large percentage of anthropogenic source contributions, however, might
63 have been supplemented by volcanic emissions and re-emission of Hg previously deposited to urban
64 surfaces in anthropogenic source regions (Rutter et al., 2009). On the other hand, TGM
65 concentrations in New York, USA (mean = 3.90 ng m⁻³) and Nanjing, China (mean = 7.9 ng m⁻³)
66 were observed to be positively correlated with air temperature and/or the intensity of solar radiation,
67 implying that land surfaces emissions contributed to elevated TGM levels (Carpi and Chen, 2002;
68 Zhu et al., 2012). This hypothesis has not considered the atmospheric transport patterns and
69 temporal variations in anthropogenic emissions at local and regional scales and needs to be further
70 validated. GOM is a potential proxy of anthropogenic sources. However, GOM has a short
71 atmospheric residence time and could be also produced via in situ oxidation of GEM, making it
72 challenging to identify the contributions of anthropogenic source to TGM or GEM in many urban
73 areas using GOM observations (Lynam and Keeler, 2005; Peterson et al., 2009; Rutter et al., 2009).
74 Relative contributions from specific sources in urban areas could be also assessed by development
75 of TGM or GEM emission inventories of different source categories. For example, total GEM
76 emissions from soils in Guiyang, China were scaled up based on an empirical model and were in
77 the similar magnitude as that from anthropogenic sources (Feng et al., 2005). Such approaches,
78 however, are very limited in many urban areas in China and other countries worldwide. Therefore,
79 the understanding of the sources of TGM or GEM in urban areas is essentially limited and there is
80 a need to develop an additional tracer to identify the controls of specific sources on the variations
81 of TGM or GEM in urban areas.

82 Hg stable isotope is a rapidly growing tool for studying the biogeochemical cycle of Hg in the
83 environments (Blum and Johnson, 2017). Hg isotopes in surface-earth system can undergo both
84 mass-dependent fractionation (MDF, $\delta^{202}\text{Hg}$ signature) and mass-independent fractionation (MIF,
85 $\Delta^{199}\text{Hg}$, $\Delta^{201}\text{Hg}$ and $\Delta^{200}\text{Hg}$ signatures), which might be caused by specific or multiple sources and
86 transformation processes (Blum et al., 2014). Previous studies found that Chinese coal-fired power
87 plants (CFPP) emitted GEM with slightly negative $\delta^{202}\text{Hg}$ (mean = -0.26‰) and significantly
88 negative $\Delta^{199}\text{Hg}$ (mean = -0.26‰) values (Tang et al., 2017; Liu et al., 2019a). Based on the
89 observed isotopic compositions of global source materials, fractionation of Hg isotopes during



90 industrial processes, and global Hg emission inventory, Sun et al. (2016b) predicted a mean $\delta^{202}\text{Hg}$
91 of -0.59‰ and a mean $\Delta^{199}\text{Hg}$ of -0.02‰ for the global primary anthropogenic GEM emissions in
92 2010. On the other hand, isotopic compositions of indoor GEM and GEM emitted from urban
93 building surface were characterized by highly negative $\delta^{202}\text{Hg}$ (means = -1.54 to -1.56‰ , $n = 2$) and
94 near-zero to slightly positive $\Delta^{199}\text{Hg}$ values (means = 0.00 to 0.17‰ , $n = 2$) (Jiskra et al., 2019a).
95 Isotopic compositions of GEM emitted from urban soils currently remain unknown. Global Hg
96 isotope models proposed this source would have highly negative $\delta^{202}\text{Hg}$ (e.g., $\sim -3.0\text{‰}$) and positive
97 $\Delta^{199}\text{Hg}$ signatures (e.g., $\sim 1.7\text{‰}$) (Sonke, 2011; Sun et al., 2019). Therefore, GEM emitted from
98 anthropogenic sources is probably isotopically distinguishable from that emitted from land surfaces
99 and indoor Hg-containing products, which provide an useful tracer for identification of TGM or
100 GEM sources in urban areas.

101 Previous studies have measured the isotopic compositions of TGM or GEM at many rural and
102 fewer urbanized sites in the Northern Hemisphere (Gratz et al., 2010; Sherman et al., 2010; Demers
103 et al., 2013; Demers et al., 2015; Enrico et al., 2016; Fu et al., 2016; Yu et al., 2016; Obrist et al.,
104 2017; Xu et al., 2017; Fu et al., 2018; Fu et al., 2019; Jiskra et al., 2019a; Jiskra et al., 2019b).
105 According to these studies, TGM or GEM isotopic compositions in urban areas showed a mean
106 $\delta^{202}\text{Hg}$ of $-0.49 \pm 0.28\text{‰}$ and a mean $\Delta^{199}\text{Hg}$ of $0.02 \pm 0.04\text{‰}$ (1σ , $n = 4$), which were much lower
107 and higher, respectively, than the mean values observed in rural areas (mean $\delta^{202}\text{Hg} = 0.56 \pm 0.45\text{‰}$,
108 mean $\Delta^{199}\text{Hg} = -0.18 \pm 0.06\text{‰}$, 1σ , $n = 10$). The lower TGM $\delta^{202}\text{Hg}$ and higher $\Delta^{199}\text{Hg}$ signatures
109 in urban areas relative to rural areas were previously hypothesized to be mainly related to primary
110 anthropogenic emissions, whereas the effect of emission and re-emission of GEM from urban
111 surfaces was frequently neglected mainly because of the poor understanding of their isotopic
112 signatures. It should be noted that many observational TGM $\delta^{202}\text{Hg}$ values in urban areas (e.g.,
113 Beijing and Guiyang of China) or in urbanized and industrial plumes were far more negative than
114 that estimated for anthropogenic emissions (-0.59‰) (Sun et al., 2016b; Yu et al., 2016; Fu et al.,
115 2018). This indicates that primary anthropogenic emissions were not the exclusive explanation for
116 the highly negative TGM $\delta^{202}\text{Hg}$ signatures in the urban atmosphere.

117 In this study, TGM concentrations and isotopic compositions were measured in ten Chinese
118 cities in summer and winter 2018, providing a unique opportunity for studying the spatial and
119 seasonal variations in TGM concentrations and isotopic compositions in urban areas of China.
120 Isotopic compositions of GEM emitted from soils were also measured in two Chinese cities, and
121 together with data in literature were used to investigate the role of land surface emissions in the
122 seasonal and spatial variations in TGM concentrations and isotopic compositions in major Chinese
123 cities. The findings in this study are helpful for a better understanding of the sources of atmospheric



124 TGM in urban areas of China, and knowledge gained emphasizes the need to mitigate surface Hg
125 emissions during implementation of the Minamata Convention.

126 **2. Methods**

127 **2.1 Study sites**

128 One sampling site in each of the ten cities was selected for measuring TGM concentrations and
129 isotopic compositions. These cities include Beijing, Shijiazhuang, Jinan in northern China, Lanzhou
130 in northwestern China, Zhengzhou and Wuhan in central China, Shanghai in eastern China,
131 Chengdu and Guiyang in southwestern China, and Guangzhou in southern China (Figure S1). Site
132 locations, information of the ten cities, and sampling periods are given in Table S1. Briefly, these
133 cities have populations of 3.75 to 21.54 million in urban areas. Fractions of the urban and buildup
134 land area out of the total land area of a $1^\circ \times 1^\circ$ grid surrounding the sampling sites ranged from 4.9%
135 to 41.1% (mean = 22.5%), whereas the remaining land surfaces are mainly croplands, barren lands,
136 open grassland, open shrublands, and open forests (range from 35.6% to 82.3% with a mean of
137 57.5%) (Figure S2 and Table S1). The sampling sites are generally located in heavily commercial
138 and residential areas in all the cities and with no major industrial Hg emission sources within 2 km
139 of the sampling sites. All the measurements were conducted on building roofs at elevations of >10
140 m. In order to investigate the shift of GEM isotopic compositions in urban areas relative to that in
141 remote areas due to local urbanized emissions, a same type of measurements was also conducted at
142 the rural Waliguan Baseline Observatory in northwestern China (Mt. Waliguan), which belongs to
143 the World Meteorological Organization's (WMO) Global Atmospheric Watch (GAW) network
144 (Figure S1).

145 **2.2 Sampling of TGM**

146 In this study, chlorine-impregnated activated carbon (CLC, 0.5 g) traps were used to collect
147 atmospheric TGM samples (Fu et al., 2014). A schematic diagram of the sampling system is shown
148 in Figure S3. Briefly, particles in ambient air were firstly removed using a Teflon filter (47 mm
149 diameter; $0.2 \mu\text{m}$ pore size) at the inlet of the sampling system, and then ambient TGM were trapped
150 onto the CLC traps at a flow rate of $\sim 2.5 \text{ L min}^{-1}$ using a Teflon coated Mini diaphragm vacuum
151 pump (N89 KTDC, KNF Inc.). The sampling flow rate was adjusted using a needle valve installed
152 at the outlet of the vacuum pump. The inlet of the sampling system was about 1.5 m above surface
153 ground. Daily (24 h) continuous sampling of TGM at each urban site lasted for approximately one
154 week in the winter and summer of 2018, respectively (Daily samples, Table S1). The wintertime
155 samplings were conducted from 5 to 15 January 2018 simultaneously in Beijing, Shijiazhuang, Jinan,
156 Lanzhou, and Zhengzhou, and from 18 to 27 January 2018 simultaneously in Shanghai, Chengdu,
157 Wuhan, Guiyang, and Guangzhou. The summertime samplings were conducted from 29 June to 7
158 July 2018 simultaneously in Shijiazhuang, Jinan, Zhengzhou, Guiyang, and Guangzhou, and from



159 27 July to 10 August 2018 simultaneously in Beijing, Lanzhou, Shanghai, Wuhan, and Chengdu.
160 TGM samples were also continuously collected from 19 November 2014 to 19 February 2015 at Mt.
161 Waliguan with a sampling duration of 10 day. After field sampling, CLC traps were sealed carefully
162 and kept in sealed polypropylene crisper before sample processing for Hg isotope analysis.

163 GOM concentrations are generally elevated in Chinese urban areas due to local primary
164 anthropogenic emissions (Fu et al., 2015). Previous studies showed that GOM measured using
165 Tekran 2537/1130/1135 system on average accounted for 0.37 to 0.50% of TGM in Guiyang,
166 Beijing, and Shanghai, China, while the daily GOM fractions in TGM ranged from 0.04 to 1.58%
167 in Guiyang (Table S2) (Fu et al., 2011; Duan et al., 2017; Zhang et al., 2019). It is likely that the
168 Tekran system could underestimate GOM concentrations by approximately 3-fold with respect to
169 that measured by other recently developed methods (e.g., cation exchange membranes (CEM) or
170 nylon membranes) (Huang et al., 2013; Gustin et al., 2015; Gustin et al., 2019). To date, GOM has
171 not been measured by CEM or nylon membranes in Chinese urban areas. If adjusting GOM
172 concentrations by a factor of 3, the above-mentioned mean GOM fractions would be increased to
173 1.1-1.5% in Guiyang, Beijing, and Shanghai, and these values are similar to those observed in Reno,
174 Nevada, USA based on the CEM method (mean GOM fraction of 2.7%) (Gustin et al., 2019). Mean
175 $\delta^{202}\text{Hg}$ and $\Delta^{199}\text{Hg}$ of TGM in urban areas of this study ranged from -0.96 to -0.24‰ and -0.12 to -
176 0.01‰, respectively. Assuming that the isotope composition of GOM resemble those of primary
177 anthropogenic emissions (e.g., $\delta^{202}\text{Hg} = -0.77\text{‰}$, $\Delta^{199}\text{Hg} = -0.06\text{‰}$) (Sun et al., 2016b), a maximum
178 GOM fraction of TGM (5%) would lead to negligible shifts in TGM $\delta^{202}\text{Hg}$ (-0.03 to 0.01‰) and
179 $\Delta^{199}\text{Hg}$ (-0.003 to 0.003‰). Therefore, TGM isotopic composition measured in this study would
180 not be biased significantly by GOM compounds. The interchange use of the terms “TGM” or “GEM”
181 in this and previous studies would not confound significantly the intercomparison of isotopic
182 composition.

183 2.3 Sample processing and TGM analysis

184 Before the analysis of Hg concentration and isotopic composition, TGM collected on CLC
185 traps were preconcentrated into 5 mL of $2\text{HNO}_3/1\text{HCl}$ mixed acid solution (40%) following
186 previous studies (Biswas et al., 2008; Sun et al., 2013; Fu et al., 2014). Trapping solution Hg
187 concentrations were measured by Tekran 2500 Hg analyzer following US EPA Method 1631
188 (USEPA, 2002). TGM concentrations of the samples were calculated using Eq. (1):

$$189 \quad \text{TGM} = \frac{C \times V_{\text{solution}}}{V_{\text{gas}}} \quad (1)$$

190 where TGM is the atmospheric TGM concentration in ng m^{-3} , C is the Hg concentration in trap
191 solution in ng mL^{-1} , V_{solution} is the volume of trap solution in mL, and V_{gas} is the cumulative sampling
192 air volume in m^3 . Full procedural blanks of field sampling and preconcentration were measured at
193 each sampling site and in each season by combustion of sealed field CLC traps (containing 0.5 g



194 CLC) prepared before field sampling. The mean Hg concentration in these sealed field blanks was
195 0.20 ± 0.09 ng (1σ , $n = 27$, Table S3), which was negligible ($<5\%$) compared to the Hg in trapping
196 solutions of samples. Breakthrough tests showed that 96.7 to 99.6% (mean = $98.9 \pm 0.9\%$, 1σ , $n =$
197 10) of TGM in ambient air could be collected by the CLC traps in our experiment setting (Table S3).
198 Recoveries of the preconcentration were tested by combustion of Lichen CRM (BCR 482), which
199 showed a mean value of $92.5 \pm 3.9\%$ (1σ , $n = 6$, Table S3). Standard additions of Hg⁰ vapor (5 to
200 25 ng, produced by SnCl₂ reduction of diluted NIST 3133 solutions) to CLC traps at the 2.5 L min⁻¹
201 sampling flow rate showed a mean recovery of $93.2 \pm 11.8\%$ (1σ , $n = 11$, Table S3) for the sampling
202 and preconcentration method. These tests indicate that the above method is reliable and efficient for
203 measuring TGM concentrations and isotopic compositions.

204 2.4 TGM isotope analysis

205 Prior to isotope analysis, the concentrations of Hg in trap solution were diluted to 0.5 or 1.0 ng
206 mL⁻¹ using the 2HNO₃/1HCl mixed acid solution (20%). Isotope ratios of Hg in diluted trap
207 solutions were measured by cold vapor-multicollector inductively coupled plasma mass
208 spectrometry (CV-MC-ICPMS) using a Nu Plasma (Nu Instruments) and a Neptune (Thermo Fisher
209 Scientific) in the Institute of Geochemistry, CAS (Guiyang, China) (Fu et al., 2019). TGM Isotopic
210 compositions were calculated following Equation (2) and (3) (Blum and Bergquist, 2007):

$$211 \quad \delta^{xxx}Hg_{TGM}(\text{‰}) = \left[\frac{\left(\frac{^{xxx}Hg}{^{198}Hg} \right)_{sample}}{\left(\frac{^{xxx}Hg}{^{198}Hg} \right)_{NIST\ 3133}} - 1 \right] \times 1000 \quad (2)$$

212 where $\delta^{xxx}Hg_{TGM}$ are the MDF signatures of TGM in per mil (‰), xxx is the mass number of Hg
213 isotopes (199, 200, 201, 202, and 204), $\left(\frac{^{xxx}Hg}{^{198}Hg} \right)_{sample}$ is the isotope ratios for TGM samples,
214 and $\left(\frac{^{xxx}Hg}{^{198}Hg} \right)_{NIST\ 3133}$ is the isotope ratios for the bracketing NIST 3133 standard (concentrations
215 matched within 10% of the sample trapping solution Hg concentrations).

$$216 \quad \Delta^{xxx}Hg_{TGM}(\text{‰}) = \delta^{xxx}Hg_{TGM} - \beta \times \delta^{202}Hg_{TGM} \quad (3)$$

217 Where $\Delta^{xxx}Hg_{TGM}$ are the MIF signatures of TGM isotopes ¹⁹⁹Hg, ²⁰⁰Hg, ²⁰¹Hg, and ²⁰⁴Hg in per mil
218 (‰), and β values are 0.252, 0.5024, 0.752, and 1.493 for isotopes ¹⁹⁹Hg, ²⁰⁰Hg, ²⁰¹Hg, and ²⁰⁴Hg,
219 respectively (Blum and Bergquist, 2007).

220 Isotopic compositions of NIST 3177 Hg standard ($n = 30$), Lichen CRM (BCR 482, $n = 6$), and
221 standard additions of NIST 3133 Hg to CLC traps ($n = 11$) (Table S3) were analyzed periodically
222 during TGM isotope analysis, and the results were consistent with previously reported values or the
223 original values of the NIST 3133 Hg standard (Table S3) (Enrico et al., 2016; Sun et al., 2016a;
224 Blum and Johnson, 2017). In the present study, we report the analytical uncertainties (2σ) of TGM



225 isotopic compositions as the 2σ values of the sample replicates when they are higher than the 2σ
226 values of standard addition of NIST 3133 Hg to CLC traps. When the 2σ values of the sample
227 replicates were lower than the standard additions of NIST 3133 Hg to CLC traps, 2σ values of the
228 standard additions of NIST 3133 Hg to CLC traps were used to represent the 2σ of TGM isotopic
229 compositions.

230

231 2.5 Ancillary Parameters

232 Data for concentrations of ozone (O_3) and carbon monoxide (CO) during the sampling periods
233 were extracted from national air quality monitoring stations (<http://106.37.208.233:20035/>) located
234 within 1.5 km of the sites, with the exception of the sampling site in Guangzhou (4.1 km).
235 Normalized difference vegetation index (NDVI) around the sampling sites ($1^\circ \times 1^\circ$) was obtained
236 from the NASA Earth Observations (NEO, <https://neo.sci.gsfc.nasa.gov/>).

237 In order to investigate the effect of soil emissions on the variations in TGM concentrations and
238 isotopic compositions, GEM exchange flux between soil and atmosphere at $1^\circ \times 1^\circ$ resolution at
239 each sampling site in July and January were extracted from the gridded land surface emission
240 inventory in China simulated for 2013, which has a spatial resolution of ~ 36 km and a monthly
241 temporal resolution (Figure S1) (Wang et al., 2016). This model established a new scheme for
242 estimating soil-atmosphere GEM flux which have taken account the effect of photochemical and
243 nonphotochemical reduction of Hg(II) in soil, diffusion of Hg^0 from soil to atmosphere, as well as
244 the temperature, moisture, organic matter contents, PH, Hg concentration, bulk density, and land
245 cover of soils, etc. [more details in Wang et al., 2016]. Note that the simulated surface emission
246 inventory does not include GEM emissions from pavement, building surface and indoor Hg-
247 containing products. These sources are in close proximity to the sampling sites (Figure S2), and
248 their effect is also interpreted in Section 3.4.

249 Daily isotopic compositions of GEM emitted from hillslope barren soil in Guiyang (114.269°
250 E, 30.488° N) and from agricultural soil in Wuhan (114.269° E, 30.488° N) from 29 July to 3 August
251 2019 and from 24 to 27 August 2019, respectively, by measuring the GEM isotopic compositions at
252 the inlet and outlet of a dynamic flux chamber, followed by a calculation based on the binary mixing
253 model (Eq. 4 and 5):

$$254 \quad \delta^{xxx}GEM_{emission} = (\delta^{xxx}GEM_{outlet} \times GEM_{outlet} - \delta^{xxx}GEM_{inlet} \times GEM_{inlet}) \div (GEM_{outlet} - GEM_{inlet}) \quad (4)$$

$$255 \quad \Delta^{xxx}GEM_{emission} = (\Delta^{xxx}GEM_{outlet} \times GEM_{outlet} - \Delta^{xxx}GEM_{inlet} \times GEM_{inlet}) \div (GEM_{outlet} - GEM_{inlet}) \quad (5)$$

256 where xxx corresponds to the mass number of Hg isotopes (199, 200, 201, 202 (not for MIF
257 signature), and 204), $\delta^{xxx}GEM_{outlet}$ and $\Delta^{xxx}GEM_{outlet}$ are the MDF and MIF values of GEM at the
258 outlet, respectively, $\delta^{xxx}GEM_{inlet}$ and $\Delta^{xxx}GEM_{inlet}$ are the MDF and MIF values of GEM at the inlet,



259 respectively, and GEM_{outlet} and GEM_{inlet} are the GEM concentrations measured at the outlet and
260 inlet, respectively.

261 3. Results and Discussion

262 3.1 TGM concentrations

263 Mean TGM concentrations at the urban sites during the study periods ranged from 2.34 to 4.56
264 $ng\ m^{-3}$ ($n = 10$) with a mean ($\pm 1\sigma$) of $3.08 \pm 0.79\ ng\ m^{-3}$ (Figure 1). These values were 1.5 to 3.0
265 times higher than the mean background value of $1.51\ ng\ m^{-3}$ in 2014 in the Northern Hemisphere
266 obtained from the Global Mercury Observation System (GMOS) (Sprovieri et al., 2016), and 1.2 to
267 2.4 times higher than the mean value of 1.94 ± 0.64 ($\pm 1\sigma$) $ng\ m^{-3}$ at urban sites in North America
268 and Europe (Mao et al., 2016). Mean TGM concentrations observed at some urban sites were,
269 however, 44-55% lower than previously reported mean values for earlier years, e.g., $4.19\ ng\ m^{-3}$ in
270 Shanghai in 2014, $8.88\ ng\ m^{-3}$ in Guiyang in 2010, and $4.60\ ng\ m^{-3}$ in Guangzhou in 2011 (Chen et
271 al., 2013; Fu and Feng, 2015; Duan et al., 2017), likely due to a combination of several factors such
272 as decreased anthropogenic emissions (Liu et al., 2019b), different sampling locations even inside
273 the same city, and different sampling times and durations of the year. The declining TGM
274 concentration (by 40%) in recent years (2014-2016) has indeed been reported in Chongming Island,
275 Shanghai (Tang et al., 2018), which has been mostly attributed to reduced anthropogenic Hg
276 emissions in China. Such emission reductions would impact more on urban than rural areas in
277 atmospheric TGM (Liu et al., 2019b).

278 3.2 TGM isotopic compositions

279 Figure 2 shows the isotopic compositions of daily TGM samples collected at the ten urban and
280 one rural sites. Large variations in daily TGM isotopic compositions were observed with values
281 ranging from -1.68 to 0.63‰ for $\delta^{202}Hg$ and from -0.23 to 0.10‰ for $\Delta^{199}Hg$ (Figure 2 and Table
282 S4). Mean TGM $\delta^{202}Hg$ values were the lowest in Guiyang ($-0.96 \pm 0.42\text{‰}$, 1σ), Lanzhou ($-0.70 \pm$
283 0.35‰ , 1σ), and Chengdu ($-0.68 \pm 0.44\text{‰}$, 1σ) in southwestern and northwestern China, followed
284 by Wuhan (mean = $-0.68 \pm 0.23\text{‰}$, 1σ) and Zhengzhou (mean = $-0.55 \pm 0.24\text{‰}$, 1σ) in central China,
285 Shijiazhuang ($-0.54 \pm 0.44\text{‰}$, 1σ) and Jinan ($-0.50 \pm 0.42\text{‰}$, 1σ) in northern China, coastal
286 Guangzhou ($-0.44 \pm 0.17\text{‰}$, 1σ) in southern China, coastal Shanghai ($-0.32 \pm 0.35\text{‰}$, 1σ) in eastern
287 China, and was the highest in Beijing ($-0.24 \pm 0.24\text{‰}$, 1σ) in Northern China (Figure 1 and Table
288 S5). Much smaller spatial variations were seen in mean TGM $\Delta^{199}Hg$ than TGM $\delta^{202}Hg$. The highest
289 mean TGM $\Delta^{199}Hg$ were observed in Guiyang ($-0.01 \pm 0.06\text{‰}$, 1σ) and Chengdu ($-0.01 \pm 0.03\text{‰}$,
290 1σ), whereas values at the other urban sites ranged from -0.12 to -0.04‰ ($n = 8$). Mean TGM $\delta^{202}Hg$
291 ($-0.16 \pm 0.16\text{‰}$, 1σ) (or $\Delta^{199}Hg = -0.10 \pm 0.04\text{‰}$, 1σ) value measured at rural Mt. Waliguan in
292 winter were higher (or lower) than that in most cities in winter, with the exception of $\delta^{202}Hg$ in



293 Beijing and Shanghai (means = -0.09 to -0.07‰, n = 2) and $\Delta^{199}\text{Hg}$ in Shijiazhuang, Jinan, and
294 Shanghai (means = -0.11 to 0.17‰, n = 3), where TGM concentrations were low (means = 1.88 to
295 2.12 ng m⁻³) and comparable to that at rural Mt. Waliguan (Table S5). Mean TGM $\Delta^{200}\text{Hg}$ values at
296 the urban sites were all indistinguishable from zero (-0.03 to 0.02‰, n = 10, Table S5), a
297 phenomenon that is similar to previous observations in urban areas in China and USA (means = -
298 0.01 to 0.01‰, n = 4) (Gratz et al., 2010; Yu et al., 2016; Xu et al., 2017). Therefore, we do not
299 further interpret the MIF of even-mass Hg isotopes in this study.

300 Mean values of TGM $\delta^{202}\text{Hg}$ and $\Delta^{199}\text{Hg}$ in this study were similar to those reported at urban
301 sites of China in previous studies, e.g., negative $\delta^{202}\text{Hg}$ (means = -0.73 to -0.08‰, n = 3) and close
302 to zero $\Delta^{199}\text{Hg}$ (means = -0.03 to 0.04‰, n = 3) in Beijing, Xi'an, and Guiyang (Yu et al., 2016; Xu
303 et al., 2017). On the other hand, mean TGM $\delta^{202}\text{Hg}$ values in this study were 0.44 to 1.60‰ lower
304 than the values reported for rural areas of China (mean = $0.20 \pm 0.40\%$, 1 σ , n = 3) and North
305 America and Europe (mean = $0.71 \pm 0.39\%$, 1 σ , n = 7), whereas mean TGM $\Delta^{199}\text{Hg}$ values were
306 0.02 to 0.18‰ higher than the means in rural areas of China (mean = $-0.14 \pm 0.05\%$, 1 σ) and North
307 America and Europe (mean = $-0.20 \pm 0.05\%$, 1 σ) (Figure 2) (Gratz et al., 2010; Demers et al., 2013;
308 Demers et al., 2015; Enrico et al., 2016; Fu et al., 2016; Obrist et al., 2017; Fu et al., 2018; Fu et al.,
309 2019; Jiskra et al., 2019b). Apparently, atmospheric TGM is isotopically distinguishable between
310 urban and rural sites and between different regions of the world, providing a potentially valuable
311 tracer for understanding the sources and transformations of atmospheric Hg at local, regional, and
312 global scales. As shown in Figure 2, some of the daily TGM isotopic compositions (i.e., $\delta^{202}\text{Hg}$ and
313 $\Delta^{199}\text{Hg}$ signatures) fell in-between the end-member TGM isotopic compositions estimated for
314 anthropogenic TGM emissions and observed from background areas, suggesting mixed influences
315 on TGM isotopic compositions between anthropogenic emissions and background atmospheric pool
316 (Demers et al., 2015; Fu et al., 2016; Xu et al., 2017; Fu et al., 2018). There were, however, many
317 exceptions with daily TGM isotopic compositions outside the above-mentioned range, e.g., with
318 $\delta^{202}\text{Hg}$ lower than -0.75‰ or $\Delta^{199}\text{Hg}$ higher than -0.01‰ (Figure 2). Thus, additional sources and
319 environmental processes should have also contributed to the variations in TGM isotopic
320 compositions in urban environments of China.

321 **3.3 TGM isotopic compositions estimated for urbanized source end-members and measured** 322 **for soil emissions**

323 Mean TGM concentrations at the urban sites (2.37 to 4.56 ng m⁻³, n = 10) were highly elevated
324 compared to the background value (~ 1.5 ng m⁻³) in the Northern Hemisphere (Sprovieri et al., 2016).
325 This could be attributed to local and regional Hg sources including Hg emissions from primary
326 anthropogenic sources, land surfaces (e.g., soil, building, and pavement), and indoor Hg-containing
327 products. As shown in Figure 2, TGM isotopic compositions in the cities were probably controlled



328 by a binary physical mixing between the regional-scale background and the key end-member
329 sources in the cities, which could be likely associated with the local and regional emission sources.
330 Here we use a linearized binary physical mixing diagram to estimate the mean isotopic signature of
331 the urbanized source end-members by extrapolating the $1/\text{TGM}_{\text{mean}}$ to zero (where TGM is mostly
332 derived from urbanized sources) (Figure 3), which showed $\delta^{202}\text{Hg}$ and $\Delta^{199}\text{Hg}$ values of
333 approximately $-1.16 \pm 0.15\text{‰}$ and $0.05 \pm 0.02\text{‰}$ (1σ), respectively.

334 The estimated $\delta^{202}\text{Hg}$ (or $\Delta^{199}\text{Hg}$) for urbanized emissions was much lower (or much higher)
335 than the $\delta^{202}\text{Hg}$ of -0.26‰ (or $\Delta^{199}\text{Hg}$ of -0.26‰) for GEM emitted from CFPP in China (Tang et
336 al., 2017; Liu et al., 2019a). The isotopic signatures of other anthropogenic emission sectors in
337 China have not been appropriately constrained. Sun et al. (2016b) estimated a mean $\delta^{202}\text{Hg}$ of -0.59‰
338 and a mean $\Delta^{199}\text{Hg}$ of -0.02‰ for the global anthropogenic GEM emissions in 2010. Our estimate
339 of $\delta^{202}\text{Hg}$ and $\Delta^{199}\text{Hg}$ for the urbanized sources were, however, 0.57‰ lower and 0.07‰ higher
340 than their predicted value for anthropogenic emissions, respectively. A recent study by Jiskra et al.
341 (2019a) showed highly negative $\delta^{202}\text{Hg}$ (means = -1.54 to -1.56‰ , $n = 2$) and high $\Delta^{199}\text{Hg}$ values
342 (means = 0.00 to 0.17‰ , $n = 2$) for GEM in air impacted by Hg emissions from building surface
343 and indoor sources, and these values seemed to support, to some extent, the estimated negative
344 $\delta^{202}\text{Hg}$ and close to zero $\Delta^{199}\text{Hg}$ signatures of urbanized sources in the present study.

345 Soil emissions are potentially an important source of atmospheric TGM in urban areas (Feng
346 et al., 2005; Agnan et al., 2016), and GEM emission fluxes from urban soils were reported to be
347 approximately one order of magnitude higher than that from pavement and building surface (Gabriel
348 et al., 2006; Eckley and Branfireun, 2008). The sampling sites in the present study were largely
349 surrounded by cropland and sparsely vegetated soils (Figure S2), and it is therefore important to
350 investigate their effects on the variations in TGM concentrations and isotopic compositions. The
351 measured mean GEM emission fluxes from soils in Guiyang and Wuhan in summer were $35.9 \pm$
352 32.6 (1σ , $n = 5$) and 9.8 ± 5.3 (1σ , $n = 3$) $\text{ng m}^{-2} \text{h}^{-1}$, respectively. The mean $\delta^{202}\text{Hg}$ and $\Delta^{199}\text{Hg}$
353 values of GEM emitted from soils were $-2.16 \pm 0.60\text{‰}$ and $-0.27 \pm 0.15\text{‰}$ (1σ , $n = 5$), respectively,
354 in Guiyang, and were $-1.07 \pm 0.86\text{‰}$ and $-0.01 \pm 0.52\text{‰}$ (1σ , $n = 3$), respectively, in Wuhan (Figure
355 S4). These values suggest that the isotopic compositions of soil GEM emissions in urban areas of
356 China likely have highly negative $\delta^{202}\text{Hg}$ values, similar to that of GEM emitted from building
357 surface and indoor Hg-containing products (Jiskra et al., 2019a). We thus hypothesize that soil,
358 building surface, and indoor Hg-containing products emissions contributed to the highly negative
359 TGM $\delta^{202}\text{Hg}$ values observed in this study. Based on the estimated $\delta^{202}\text{Hg}$ values of urbanized
360 source end-member (mean = -1.16‰), anthropogenic emissions (mean = -0.59‰), and GEM
361 emitted from soils, building surface and indoor Hg-containing products (mean = -1.57‰) in this
362 and previous studies (Sun et al., 2016b; Jiskra et al., 2019a), we estimate that the contribution of



363 soil, building surface and indoor Hg-containing products emissions to the TGM in the ten cities was
364 approximately equal to that of primary anthropogenic emissions (48% versus 52%). We caution that,
365 due to the fact that the isotopic signatures of GEM emitted from many anthropogenic sources and
366 land surfaces in China have not been well constrained, such a preliminary assessment should have
367 large uncertainties. However, our estimate is overall consistent with previous studies on GEM
368 emission fluxes from land surfaces and anthropogenic sources in Chinese urban areas. For example,
369 Previous studies on GEM emission fluxes from urban surfaces in China showed a mean value of
370 $83.2 \pm 170 \text{ ng m}^{-2} \text{ h}^{-1}$ (1σ , $n = 39$) (Fang et al., 2004; Feng et al., 2005; Wang et al., 2006; Fu et al.,
371 2012), which was relatively higher than the mean anthropogenic GEM flux ($48.4 \pm 48.1 \text{ ng m}^{-2} \text{ h}^{-1}$,
372 1σ , $n = 10$) in the ten investigated cities (Table S5) (AMAP/UNEP, 2013). The findings in this and
373 previous studies therefore suggest that soil, building surface, and indoor Hg-containing products
374 emissions would play an important role in regulating the TGM concentrations and isotopic
375 compositions in urban areas of China, which is further discussed in the following section.

376 **3.4 Effect of surface emissions on seasonal variations in TGM concentrations and isotopic** 377 **compositions**

378 Strong seasonal variations in the mean TGM concentrations and isotopic compositions were
379 observed for most cities (Figure 4). The mean TGM concentrations and $\Delta^{199}\text{Hg}$ values were
380 relatively higher in summer than winter in most cities except for the two (Guiyang and Guangzhou)
381 in the low latitudes that showed an opposite trend. On the contrary, the mean TGM $\delta^{202}\text{Hg}$ showed
382 lower values in summer than winter in all the cities except southernmost Guangzhou that showed
383 no seasonal difference. The seasonal variations in TGM concentrations and $\delta^{202}\text{Hg}$ in the present
384 study were consistent with previous findings generated from year-round continuous observations in
385 China, e.g., higher summertime TGM in Beijing and Shanghai (Zhang et al., 2013; Duan et al.,
386 2017), higher wintertime TGM in Guiyang and Guangzhou (Feng et al., 2004; Chen et al., 2013),
387 and lower summer $\delta^{202}\text{Hg}$ in Guiyang and Xi'an (Yu et al., 2016; Xu et al., 2017).

388 The summertime higher TGM concentrations observed in most cities in the present study was
389 in contrast to the observations in most rural areas in China as well as in other regions in the Northern
390 Hemisphere, which frequently showed lower TGM or GEM concentrations in summer than in
391 winter (Fu et al., 2015; Mao et al., 2016; Jiskra et al., 2018). Studies on the seasonal variations in
392 TGM or GEM isotopic compositions in rural areas are currently limited. A recent study at rural Mt.
393 Changbai, northeastern China showed higher TGM $\delta^{202}\text{Hg}$ values in summer than winter (Fu et al.,
394 2019), which is opposite to the seasonal variations in TGM $\delta^{202}\text{Hg}$ at most urban sites in the present
395 study. Such a summertime lower TGM or GEM and higher $\delta^{202}\text{Hg}$ pattern in rural areas should be
396 mainly attributed to increasing atmospheric oxidation and vegetation uptake of GEM as well as
397 decreasing residential coal combustion (Sprovieri et al., 2016; Horowitz et al., 2017; Jiskra et al.,



398 2018; Fu et al., 2019; Sun et al., 2019). The seasonality in atmospheric oxidation chemistry,
399 vegetation activity and residential coal combustion should be similar between urban and rural areas
400 in China, as reflected by the seasonality in O₃ (representing atmospheric oxidation chemistry),
401 NDVI (representing vegetation activity), and CO (dominantly (40%) originates from residential coal
402 combustion) (Jiskra et al., 2018; Zheng et al., 2018), which showed summertime higher O₃
403 concentrations and NDVI and lower CO concentrations at most urban sites (Figure S5). Therefore,
404 the contrasting seasonal variations in TGM concentrations and isotopic compositions at most urban
405 sites with respect to rural sites provided evidence that summertime enhanced emissions in these
406 cities probably outbalanced the effect of seasonal variations in atmospheric oxidation chemistry,
407 vegetation activity, and residential coal combustion.

408 Traditionally, local and regional anthropogenic emissions are thought to dominate the TGM or
409 GEM pollution in urban areas of China (Lin et al., 2010). A recent study showed quantitatively
410 comparable coal combustion Hg emission in China between winter and summer (Gao et al., 2019).
411 Seasonal-resolution Hg emission inventories for other anthropogenic sources (e.g., productions of
412 cement, iron and steel, aluminum and non-ferrous metals) in China have not been established. Based
413 on the monthly production data of these source materials, we estimated that there is no strong
414 seasonality in total Hg emissions from these sources (Table S6). Prevailing wind directions during
415 the wintertime and summertime sampling campaigns were similar Jinan, Lanzhou, Zhengzhou, and
416 Shanghai, but were different in other remaining cities (Figure S6). Variations in predominant wind
417 directions would change the relationships between receptor and regional anthropogenic emissions,
418 which could further influence the TGM levels and isotopic compositions in these cities. Given the
419 similarity in wintertime and summertime prevailing wind directions in some cities and consistent
420 summertime lower CO concentrations in most cities, it is postulated that the variations in local
421 anthropogenic emissions and transport of regional anthropogenic emissions were not likely the main
422 cause for the seasonal variations in TGM concentrations and isotopic compositions.

423 We found that the amplitudes of seasonal variations in TGM concentrations ($(TGM_{\text{summer}} -$
424 $TGM_{\text{winter}})/TGM_{\text{summer}}$) and $\Delta^{199}\text{Hg}$ values ($\Delta^{199}\text{Hg}_{\text{summer}} - \Delta^{199}\text{Hg}_{\text{winter}}$) were both significantly
425 positively correlated with latitude of the cities (ANOVA, R² were 0.85 and 0.66 for TGM and
426 $\Delta^{199}\text{Hg}$, respectively, $p < 0.01$ for both, Figure 5A and C), whereas the seasonal $\delta^{202}\text{Hg}$ amplitudes
427 ($\delta^{202}\text{Hg}_{\text{summer}} - \delta^{202}\text{Hg}_{\text{winter}}$) were significantly negatively correlated with latitude (ANOVA, R² =
428 0.46, $p < 0.01$, Figure 5B). This indicates the seasonality in TGM concentrations and isotopic
429 compositions were likely related to weather- and climate-dependent (e.g., solar radiation and air
430 temperature) sources and/or atmospheric processes.

431 GEM emission fluxes from soil, building surface and pavement in urban areas are highly
432 related to solar radiation and temperature and frequently peak in summer in the Northern



433 Hemisphere (Gabriel et al., 2006; Eckley and Branfireun, 2008). Studies on the seasonal variations
434 in GEM emissions from building surface and pavement are not available in Chinese urban areas,
435 but are expected to be similar to that of soil GEM emission (Gabriel et al., 2006). Therefore, using
436 simulated seasonal soil GEM emission data is generally adequate to interpret the effect of surface
437 GEM emission on the seasonal variations in TGM concentrations and isotopic compositions. As
438 shown in Figure 6A, a significant positive correlation was observed between the seasonal
439 amplitudes of TGM concentration and simulated soil GEM emission flux ($(\text{flux}_{\text{July}} -$
440 $\text{flux}_{\text{January}})/\text{flux}_{\text{July}}$), indicating enhanced surface GEM emission is responsible for the summertime
441 increase of TGM concentrations at most urban sites. Negative seasonal TGM magnitudes were
442 observed in Guiyang and Guangzhou in the low latitudes where there is a small summertime
443 increase of soil GEM emission fluxes (Figure 6A). We postulate that the effect of surface emission
444 on the seasonal variations in TGM concentrations in Guiyang and Guangzhou was likely
445 outbalanced by other factors, e.g., seasonal variations in atmospheric oxidization chemistry,
446 vegetation activity, and residential coal combustion.

447 Site-specific mean TGM $\delta^{202}\text{Hg}$ and $\Delta^{199}\text{Hg}$ values were calculated for summer and winter
448 sampling campaigns separately, and then values at all the sampling sites were correlated with their
449 respective simulated soil GEM emission fluxes. A significant negative correlation was obtained
450 between TGM $\delta^{202}\text{Hg}$ and simulated soil emission (ANOVA, $R^2 = 0.43$, $p < 0.01$, Figure 6B). As
451 mentioned above, the isotopic compositions of GEM emitted from urban surfaces were
452 characterized by highly negative $\delta^{202}\text{Hg}$ values (mean = -1.57%). Thus, high surface GEM
453 emissions should shift TGM $\delta^{202}\text{Hg}$ towards negative values. A weak positive correlation was
454 observed between mean TGM $\Delta^{199}\text{Hg}$ and simulated soil GEM emission fluxes (ANOVA, $R^2 = 0.21$,
455 $p < 0.05$, Figure 6B), suggesting that high surface GEM emissions led to a slightly positive shift of
456 TGM $\Delta^{199}\text{Hg}$. Seasonal amplitudes of $\delta^{202}\text{Hg}$ (or $\Delta^{199}\text{Hg}$) in the ten cities were significantly
457 negatively (or positively) correlated with seasonal amplitudes of simulated soil GEM emission flux
458 (ANOVA, R^2 of 0.54 or 0.63, $p < 0.01$ for both, Figure S7), suggesting the dominant role of surface
459 GEM emissions on the seasonal variations in TGM isotopic compositions.

460 It should be noted that indoor TGM also have highly negative $\delta^{202}\text{Hg}$ (-1.56% , $n = 1$) and
461 positive $\Delta^{199}\text{Hg}$ (0.17% , $n = 1$) values (Jiskra et al., 2019a), but this source is not likely a dominant
462 one contributing to the seasonal variations in TGM isotopic compositions. Indoor TGM
463 concentrations in urban areas can be highly elevated mainly due to evaporation of GEM from Hg-
464 containing products (e.g., spills of liquid mercury in thermometers, fluorescent light and Hg
465 switches) in the absence of sunlight (Carpi and Chen, 2001; Baughman, 2006). This source is
466 expected to yield $\Delta^{199}\text{Hg}/\Delta^{201}\text{Hg}$ slopes of ~ 1.6 in TGM isotopic compositions due to nuclear
467 volume effect (NVE) (Zheng and Hintelmann, 2010; Ghosh et al., 2013). As shown in Figure S8, a



468 York bivariate linear regression between TGM $\Delta^{199}\text{Hg}$ and $\Delta^{201}\text{Hg}$ in the studied cites showed a
469 slope of 1.01 ± 0.10 (1σ), which is consistent with that of soil GEM emissions (1.09 ± 0.06 , 1σ , Figure
470 S7) and that of photoreduction of Hg(II) to GEM (~ 1.0) (Blum et al., 2014), but much lower than
471 that predicted for indoor GEM sources, suggesting that seasonal variations in TGM isotopic
472 compositions were unlikely dominated by indoor emission sources.

473 Hence, we can conclude that the seasonal variations in TGM concentrations and isotopic
474 compositions in the ten cities were likely controlled by surface emission sources. However, it is
475 currently difficult to determine which of surface emission sources (e.g., soil, pavement, or building
476 surface) was more important. As discussed earlier, GEM emitted from these sources were
477 characterized by similar isotopic signatures and are difficult to be distinguished. GEM emissions
478 flux data from pavement and building surface in Chinese urban areas are very limited. A previous
479 study in Toronto, Canada and Austin, USA reported that GEM emission fluxes from soils were on
480 average 8 times higher than those from pavement and building surface (Eckley and Branfireun,
481 2008). This, together with the large fraction of cropland and sparsely vegetated soils area in the total
482 urban land area (mean = 57%, Table S1), indicates soil emissions were likely more important than
483 building surface and pavement emissions at a regional scale (e.g., the size of $1^\circ \times 1^\circ$ surrounding the
484 sampling sites). However, given that building surface and pavement emissions sources were in close
485 proximity to the sampling sites (Figure S2), their contributions to atmospheric TGM budget may
486 exceed those of soil emission sources locally. Therefore, further studies and approaches are needed
487 to better constrain the contributions of local and regional land surface emissions to TGM variations
488 at specific sites.

489 3.5 Conclusions and implications

490 TGM concentrations in Chinese urban areas were generally highly elevated, which was
491 traditionally thought to be mainly attributed to primary anthropogenic emissions (Lin et al., 2010;
492 Fu et al., 2015). Due to the implementation of aggressive air pollution control measures in China
493 since 2014, primary anthropogenic Hg emissions within or surrounding many Chinese cities are
494 expected to have been reduced noticeably in recent years (Liu et al., 2019b). Land surface Hg
495 emissions are also an important source of atmospheric Hg (Selin et al., 2007; Holmes et al., 2010;
496 Pirrone et al., 2010; Agnan et al., 2016). Therefore, questions have emerged as to whether land
497 surface emissions become important in the variations in TGM concentrations and isotopic
498 compositions in Chinese urban areas. The present study suggests that surface GEM emissions likely
499 dominated the seasonal variations in TGM concentrations and isotopic compositions in most cities.
500 GEM emissions from land surface are generally higher in summer and characterized by significantly
501 negative $\delta^{202}\text{Hg}$ signatures, and therefore are able to cause increasing TGM concentrations and a
502 negative shift of TGM $\delta^{202}\text{Hg}$ in summer in Chinese cities. Therefore, we suggest that land surface



503 emissions should be incorporated in future studies to interpret the cycling (or fractionation) of TGM
504 (or TGM isotopes) in urban areas and/or other regions with strong land surface GEM emissions.

505 China has been regarded as the world's strongest source region of anthropogenic Hg emissions.
506 Since the Chinese Economic Reform in 1978, more than 13000 Mg of Hg have been released into
507 the atmosphere from anthropogenic sources (Wu et al., 2016). Large fractions (35 to 49%) of these
508 emitted Hg were in the form of short-lived particulate bound and oxidized Hg, and would have
509 deposited quickly to areas close to sources such as urbanized and industrial areas, which should
510 have increased Hg contents in land surface substrates. The combining effects of global warming and
511 increased substrate Hg contents would induce increasing surface emissions, blunting the benefits of
512 anthropogenic Hg emission control in China. Therefore, future studies should be conducted in
513 systematically assessing the negative effects of increasing soil Hg emissions in a changing
514 environment (anthropogenic emission, climate, and land use change) during the implementation of
515 the Minamata Convention. Possible strategies should also be considered to mitigate surface Hg
516 emissions, and together with the effective controls of anthropogenic emissions, to eventually reduce
517 the threats of Hg to human health and the environment.

518 **Data Availability:**

519 All the dataset used in this study can be found in Supporting information.

520 **Author contribution:**

521 X.W.F., G.Z., J.L., H.G., and X.B.F. initiated the project and designated the field experiments.
522 X.W.F., C.L., H.Z., Y.X., H.Z., X.P.L. carried out the field sampling. C.L. and H.Z. performed the
523 laboratory analysis. X.W.F. prepared the manuscript with contributions from all co-authors.

524 **Acknowledgements:**

525 This work was funded by the “National Key R&D Program of China (2017YFC0212001)”, the
526 Chinese Academy of Sciences (ZDBS-LY-DQC029 and 2017443), the National Nature Science
527 Foundation of China (41622305), and the K.C. Wong Education Foundation. We also thank
528 Guangcai Zhong, Shuhao Dong, Baoxin Li, Shizhen Zhao, Bolun Zhang, Jiao Tang, Hongxing Jiang,
529 Buqing Xu, Yu Wang, Dawen Yao, Fengwen Huang, Kun Nie, Lingxi Zhan, Jiaying Wang, Liuyuan
530 Zhao, and Zhanxiang Wang who have contributed to the sampling of TGM.

531 **Competing interests:**

532 The authors declare that they have no conflict of interest.

533 **Supporting information:**



- 534 • Supporting Information Figure S1-S8
535 • Supporting Information Table S1-S6

536

537 **References:**

- 538 Agnan, Y., Le Dantec, T., Moore, C. W., Edwards, G. C., and Obrist, D.: New Constraints on Terrestrial
539 Surface Atmosphere Fluxes of Gaseous Elemental Mercury Using a Global Database,
540 Environmental Science & Technology, 50, 507-524, 10.1021/acs.est.5b04013, 2016.
- 541 AMAP/UNEP: Geospatially distributed mercury emissions dataset 2010v1, in, 2013.
- 542 Baughman, T. A.: Elemental mercury spills, Environ Health Persp, 114, 147-152, 10.1289/ehp.7048,
543 2006.
- 544 Biswas, A., Blum, J. D., Bergquist, B. A., Keeler, G. J., and Xie, Z. Q.: Natural mercury isotope variation
545 in coal deposits and organic soils, Environmental Science & Technology, 42, 8303-8309, Doi
546 10.1021/Es801444b, 2008.
- 547 Blum, J. D., and Bergquist, B. A.: Reporting of variations in the natural isotopic composition of mercury,
548 Anal Bioanal Chem, 388, 353-359, DOI 10.1007/s00216-007-1236-9, 2007.
- 549 Blum, J. D., Sherman, L. S., and Johnson, M. W.: Mercury isotopes in earth and environmental sciences,
550 Annu Rev Earth Pl Sc, 42, 249-269, 10.1146/annurev-earth-050212-124107, 2014.
- 551 Blum, J. D., and Johnson, M. W.: Recent Developments in Mercury Stable Isotope Analysis, Reviews in
552 Mineralogy & Geochemistry, 82, 733-757, 2017.
- 553 Carpi, A., and Chen, Y.-f.: Gaseous Elemental Mercury as an Indoor Air Pollutant, Environmental Science
554 & Technology, 35, 4170-4173, 10.1021/es010749p, 2001.
- 555 Carpi, A., and Chen, Y. F.: Gaseous elemental mercury fluxes in New York City, Water Air Soil Poll, 140,
556 371-379, Doi 10.1023/A:1020198025725, 2002.
- 557 Chen, L. G., Liu, M., Xu, Z. C., Fan, R. F., Tao, J., Chen, D. H., Zhang, D. Q., Xie, D. H., and Sun, J. R.:
558 Variation trends and influencing factors of total gaseous mercury in the Pearl River Delta-A
559 highly industrialised region in South China influenced by seasonal monsoons, Atmos Environ,
560 77, 757-766, DOI 10.1016/j.atmosenv.2013.05.053, 2013.
- 561 Demers, J. D., Blum, J. D., and Zak, D. R.: Mercury isotopes in a forested ecosystem: Implications for
562 air-surface exchange dynamics and the global mercury cycle, Global Biogeochem Cy, 27, 222-
563 238, Doi 10.1002/Gbc.20021, 2013.
- 564 Demers, J. D., Sherman, L. S., Blum, J. D., Marsik, F. J., and Dvonch, J. T.: Coupling atmospheric mercury
565 isotope ratios and meteorology to identify sources of mercury impacting a coastal urban-
566 industrial region near Pensacola, Florida, USA, Global Biogeochem Cy, 29, 1689-1705, 2015.
- 567 Duan, L., Wang, X. H., Wang, D. F., Duan, Y. S., Cheng, N., and Xiu, G. L.: Atmospheric mercury speciation
568 in Shanghai, China, Sci Total Environ, 578, 460-468, 2017.
- 569 Eckley, C. S., and Branfireun, B.: Gaseous mercury emissions from urban surfaces: Controls and
570 spatiotemporal trends, Appl Geochem, 23, 369-383,
571 <https://doi.org/10.1016/j.apgeochem.2007.12.008>, 2008.
- 572 Enrico, M., Le Roux, G., Maruszczak, N., Heimburger, L. E., Claustres, A., Fu, X. W., Sun, R. Y., and Sonke,
573 J. E.: Atmospheric Mercury Transfer to Peat Bogs Dominated by Gaseous Elemental Mercury
574 Dry Deposition, Environmental Science & Technology, 50, 2405-2412,
575 10.1021/acs.est.5b06058, 2016.
- 576 Fang, F. M., Wang, Q. C., and Li, J. F.: Urban environmental mercury in Changchun, a metropolitan city
577 in Northeastern China: source, cycle, and fate, Sci Total Environ, 330, 159-170, DOI



- 578 10.1016/j.scitotenv.2004.04.006, 2004.
- 579 Feng, X. B., Shang, L. H., Wang, S. F., Tang, S. L., and Zheng, W.: Temporal variation of total gaseous
580 mercury in the air of Guiyang, China, *J Geophys Res-Atmos*, 109, Artn D03303, Doi
581 10.1029/2003jd004159, 2004.
- 582 Feng, X. B., Wang, S. F., Qiu, G. A., Hou, Y. M., and Tang, S. L.: Total gaseous mercury emissions from
583 soil in Guiyang, Guizhou, China, *J Geophys Res-Atmos*, 110, Artn D14306, Doi
584 10.1029/2004jd005643, 2005.
- 585 Fu, X., Yang, X., Tan, Q., Ming, L., Lin, T., Lin, C.-J., Li, X., and Feng, X.: Isotopic Composition of Gaseous
586 Elemental Mercury in the Marine Boundary Layer of East China Sea, *Journal of Geophysical
587 Research: Atmospheres*, 123, 7656-7669, 10.1029/2018JD028671, 2018.
- 588 Fu, X., Zhang, H., Liu, C., Zhang, H., Lin, C.-J., and Feng, X.: Significant Seasonal Variations in Isotopic
589 Composition of Atmospheric Total Gaseous Mercury at Forest Sites in China Caused by
590 Vegetation and Mercury Sources, *Environmental Science & Technology*, 53, 13748-13756,
591 10.1021/acs.est.9b05016, 2019.
- 592 Fu, X. W., Feng, X. B., Qiu, G. L., Shang, L. H., and Zhang, H.: Speciated atmospheric mercury and its
593 potential source in Guiyang, China, *Atmos Environ*, 45, 4205-4212, DOI
594 10.1016/j.atmosenv.2011.05.012, 2011.
- 595 Fu, X. W., Feng, X. B., Zhang, H., Yu, B., and Chen, L. G.: Mercury emissions from natural surfaces highly
596 impacted by human activities in Guangzhou province, South China, *Atmos Environ*, 54, 185-
597 193, DOI 10.1016/j.atmosenv.2012.02.008, 2012.
- 598 Fu, X. W., Heimbürger, L. E., and Sonke, J. E.: Collection of atmospheric gaseous mercury for stable
599 isotope analysis using iodine- and chlorine-impregnated activated carbon traps, *J Anal Atom
600 Spectrom*, 29, 841-852, Doi 10.1039/C3ja50356a, 2014.
- 601 Fu, X. W., and Feng, X. B.: Variations of atmospheric total gaseous mercury concentrations for the
602 sampling campaigns of 2001/2002 and 2009/2010 and implications of changes in regional
603 emissions of atmospheric mercury, *Bull Miner Petr Geochem*, in press (in Chinese), 2015.
- 604 Fu, X. W., Zhang, H., Yu, B., Wang, X., Lin, C. J., and Feng, X. B.: Observations of atmospheric mercury
605 in China: a critical review, *Atmos Chem Phys*, 15, 9455-9476, 10.5194/acp-15-9455-2015, 2015.
- 606 Fu, X. W., Maruszczak, N., Wang, X., Gheusi, F., and Sonke, J. E.: Isotopic Composition of Gaseous
607 Elemental Mercury in the Free Troposphere of the Pic du Midi Observatory, France,
608 *Environmental Science & Technology*, 50, 5641-5650, 10.1021/acs.est.6b00033, 2016.
- 609 Gabriel, M. C., Williamson, D. G., Zhang, H., Brooks, S., and Lindberg, S.: Diurnal and seasonal trends
610 in total gaseous mercury flux from three urban ground surfaces, *Atmos Environ*, 40, 4269-4284,
611 DOI 10.1016/j.atmosenv.2006.04.004, 2006.
- 612 Gao, W. D., Jiang, W., and Zhou, M. M.: The spatial and temporal characteristics of mercury emission
613 from coal combustion in China during the year 2015, *Atmos Pollut Res*, 10, 776-783,
614 10.1016/j.apr.2018.12.005, 2019.
- 615 Ghosh, S., Schauble, E. A., Couloume, G. L., Blum, J. D., and Bergquist, B. A.: Estimation of nuclear
616 volume dependent fractionation of mercury isotopes in equilibrium liquid-vapor evaporation
617 experiments, *Chem Geol*, 336, 5-12, 2013.
- 618 Gratz, L. E., Keeler, G. J., Blum, J. D., and Sherman, L. S.: Isotopic composition and fractionation of
619 mercury in Great Lakes precipitation and ambient air, *Environmental Science & Technology*, 44,
620 7764-7770, Doi 10.1021/Es100383w, 2010.
- 621 Gustin, M. S., Amos, H. M., Huang, J., Miller, M. B., and Heidecorn, K.: Measuring and modeling



- 622 mercury in the atmosphere: a critical review, *Atmos Chem Phys*, 15, 5697-5713, DOI
623 10.5194/acp-15-5697-2015, 2015.
- 624 Gustin, M. S., Dunham-Cheatham, S. M., and Zhang, L.: Comparison of 4 Methods for Measurement of
625 Reactive, Gaseous Oxidized, and Particulate Bound Mercury, *Environmental Science &
626 Technology*, 53, 14489-14495, 10.1021/acs.est.9b04648, 2019.
- 627 Holmes, C. D., Jacob, D. J., Corbitt, E. S., Mao, J., Yang, X., Talbot, R., and Slemr, F.: Global atmospheric
628 model for mercury including oxidation by bromine atoms, *Atmos Chem Phys*, 10, 12037-12057,
629 DOI 10.5194/acp-10-12037-2010, 2010.
- 630 Horowitz, H. M., Jacob, D. J., Zhang, Y. X., Dibble, T. S., Slemr, F., Amos, H. M., Schmidt, J. A., Corbitt, E.
631 S., Marais, E. A., and Sunderland, E. M.: A new mechanism for atmospheric mercury redox
632 chemistry: implications for the global mercury budget, *Atmos Chem Phys*, 17, 6353-6371, 2017.
- 633 Huang, J. Y., Miller, M. B., Weiss-Penzias, P., and Gustin, M. S.: Comparison of gaseous oxidized Hg
634 measured by KCl-coated denuders, and Nylon and Cation exchange Membranes,
635 *Environmental Science & Technology*, 47, 7307-7316, Doi 10.1021/Es4012349, 2013.
- 636 Jiskra, M., Sonke, J. E., Obrist, D., Bieser, J., Ebinghaus, R., Myhre, C. L., Pfaffhuber, K. A., Wangberg, I.,
637 Kyllonen, K., Worthy, D., Martin, L. G., Labuschagne, C., Mkololo, T., Ramonet, M., Magand, O.,
638 and Dommergue, A.: A vegetation control on seasonal variations in global atmospheric
639 mercury concentrations, *Nat Geosci*, 11, 244-+, 10.1038/s41561-018-0078-8, 2018.
- 640 Jiskra, M., Maruszczak, N., Leung, K. H., Hawkins, L., Prestbo, E., and Sonke, J. E.: Automated Stable
641 Isotope Sampling of Gaseous Elemental Mercury (ISO-GEM): Insights into GEM Emissions from
642 Building Surfaces, *Environmental Science & Technology*, 53, 4346-4354,
643 10.1021/acs.est.8b06381, 2019a.
- 644 Jiskra, M., Sonke, J. E., Agnan, Y., Helmig, D., and Obrist, D.: Insights from mercury stable isotopes on
645 terrestrial-atmosphere exchange of Hg(0) in the Arctic tundra, *Biogeosciences*, 16, 4051-4064,
646 10.5194/bg-16-4051-2019, 2019b.
- 647 Lin, C. J., Pan, L., Streets, D. G., Shetty, S. K., Jang, C., Feng, X., Chu, H. W., and Ho, T. C.: Estimating
648 mercury emission outflow from East Asia using CMAQ-Hg, *Atmos Chem Phys*, 10, 1853-1864,
649 2010.
- 650 Liu, H. W., Diao, X., Yu, B., Shi, J. B., Liu, Q., Yin, Y. G., Hu, L. G., Yuan, C. G., and Jiang, G. B.: Effect of air
651 pollution control devices on mercury isotopic fractionation in coal-fired power plants, *Chem
652 Geol*, 517, 1-6, 10.1016/j.chemgeo.2019.04.019, 2019a.
- 653 Liu, K. Y., Wu, Q. R., Wang, L., Wang, S. X., Liu, T. H., Ding, D., Tang, Y., Li, G. L., Tian, H. Z., Duan, L.,
654 Wang, X., Fu, X. W., Feng, X. B., and Hao, J. M.: Measure-Specific Effectiveness of Air Pollution
655 Control on China's Atmospheric Mercury Concentration and Deposition during 2013-2017,
656 *Environmental Science & Technology*, 53, 8938-8946, 10.1021/acs.est.9b02428, 2019b.
- 657 Lyman, S. N., and Jaffe, D. A.: Formation and fate of oxidized mercury in the upper troposphere and
658 lower stratosphere, *Nat Geosci*, 5, 114-117, 10.1038/NGEO1353, 2012.
- 659 Lynam, M. M., and Keeler, G. J.: Automated speciated mercury measurements in Michigan,
660 *Environmental Science & Technology*, 39, 9253-9262, Doi 10.1021/Es040458r, 2005.
- 661 Mao, H. T., Cheng, I., and Zhang, L. M.: Current understanding of the driving mechanisms for
662 spatiotemporal variations of atmospheric speciated mercury: a review, *Atmos Chem Phys*, 16,
663 12897-12924, 2016.
- 664 Obrist, D., Agnan, Y., Jiskra, M., Olson, C. L., Colegrove, D. P., Hueber, J., Moore, C. W., Sonke, J. E., and
665 Helmig, D.: Tundra uptake of atmospheric elemental mercury drives Arctic mercury pollution,



- 666 Nature, 547, 201-204, 10.1038/nature22997, 2017.
- 667 Obrist, D., Kirk, J. L., Zhang, L., Sunderland, E. M., Jiskra, M., and Selin, N. E.: A review of global
668 environmental mercury processes in response to human and natural perturbations: Changes
669 of emissions, climate, and land use, *Ambio*, 47, 116-140, 10.1007/s13280-017-1004-9, 2018.
- 670 Peterson, C., Gustin, M., and Lyman, S.: Atmospheric mercury concentrations and speciation measured
671 from 2004 to 2007 in Reno, Nevada, USA, *Atmos Environ*, 43, 4646-4654, DOI
672 10.1016/j.atmosenv.2009.04.053, 2009.
- 673 Pirrone, N., Cinnirella, S., Feng, X., Finkelman, R. B., Friedli, H. R., Leaner, J., Mason, R., Mukherjee, A.
674 B., Stracher, G. B., Streets, D. G., and Telmer, K.: Global mercury emissions to the atmosphere
675 from anthropogenic and natural sources, *Atmos Chem Phys*, 10, 5951-5964, DOI 10.5194/acp-
676 10-5951-2010, 2010.
- 677 Rutter, A. P., Snyder, D. C., Stone, E. A., Schauer, J. J., Gonzalez-Abraham, R., Molina, L. T., Marquez, C.,
678 Cardenas, B., and de Foy, B.: In situ measurements of speciated atmospheric mercury and the
679 identification of source regions in the Mexico City Metropolitan Area, *Atmos Chem Phys*, 9,
680 207-220, 2009.
- 681 Selin, N. E., Jacob, D. J., Park, R. J., Yantosca, R. M., Strode, S., Jaegle, L., and Jaffe, D.: Chemical cycling
682 and deposition of atmospheric mercury: Global constraints from observations, *J Geophys Res-
683 Atmos*, 112, 1-14, Artn D02308, Doi 10.1029/2006jd007450, 2007.
- 684 Shah, V., Jaegle, L., Gratz, L. E., Ambrose, J. L., Jaffe, D. A., Selin, N. E., Song, S., Campos, T. L., Flocke, F.
685 M., Reeves, M., Stechman, D., Stell, M., Festa, J., Stutz, J., Weinheimer, A. J., Knapp, D. J.,
686 Montzka, D. D., Tyndall, G. S., Apel, E. C., Hornbrook, R. S., Hills, A. J., Riemer, D. D., Blake, N. J.,
687 Cantrell, C. A., and Mauldin, R. L.: Origin of oxidized mercury in the summertime free
688 troposphere over the southeastern US, *Atmos Chem Phys*, 16, 1511-1530, 10.5194/acp-16-
689 1511-2016, 2016.
- 690 Sherman, L. S., Blum, J. D., Johnson, K. P., Keeler, G. J., Barres, J. A., and Douglas, T. A.: Mass-
691 independent fractionation of mercury isotopes in Arctic snow driven by sunlight, *Nat Geosci*,
692 3, 173-177, Doi 10.1038/Ngeo758, 2010.
- 693 Sonke, J. E.: A global model of mass independent mercury stable isotope fractionation, *Geochim
694 Cosmochim Acta*, 75, 4577-4590, DOI 10.1016/j.gca.2011.05.027, 2011.
- 695 Sprovieri, F., Pirrone, N., Bencardino, M., D'Amore, F., Carbone, F., Cinnirella, S., Mannarino, V., Landis,
696 M., Ebinghaus, R., Weigelt, A., Brunke, E. G., Labuschagne, C., Martin, L., Munthe, J., Wangberg,
697 I., Artaxo, P., Morais, F., Barbosa, H. D. J., Brito, J., Cairns, W., Barbante, C., Dieguez, M. D.,
698 Garcia, P. E., Dommergue, A., Angot, H., Magand, O., Skov, H., Horvat, M., Kotnik, J., Read, K.
699 A., Neves, L. M., Gawlik, B. M., Sena, F., Mashyanov, N., Obolkin, V., Wip, D., Bin Feng, X., Zhang,
700 H., Fu, X. W., Ramachandran, R., Cossa, D., Knoery, J., Maruszczak, N., Nerentorp, M., and
701 Norstrom, C.: Atmospheric mercury concentrations observed at ground-based monitoring sites
702 globally distributed in the framework of the GMOS network, *Atmos Chem Phys*, 16, 11915-
703 11935, 2016.
- 704 Sun, G., Sommar, J., Feng, X., Lin, C.-J., Ge, M., Wang, W., Yin, R., Fu, X., and Shang, L.: Mass-dependent
705 and -independent fractionation of mercury isotope during gas-phase oxidation of elemental
706 mercury vapor by atomic Cl and Br, *Environmental Science & Technology*, 50, 9232-9241,
707 10.1021/acs.est.6b01668, 2016a.
- 708 Sun, R. Y., Enrico, M., Heimbürger, L. E., Scott, C., and Sonke, J. E.: A double-stage tube furnace-acid-
709 trapping protocol for the pre-concentration of mercury from solid samples for isotopic analysis,



- 710 Anal Bioanal Chem, 405, 6771-6781, DOI 10.1007/s00216-013-7152-2, 2013.
- 711 Sun, R. Y., Streets, D. G., Horowitz, H. M., Amos, H. M., Liu, G. J., Perrot, V., Toutain, J. P., Hintelmann,
712 H., Sunderland, E. M., and Sonke, J. E.: Historical (1850–2010) mercury stable isotope inventory
713 from anthropogenic sources to the atmosphere, *Elem. Sci. Anth*, 4, 1-15,
714 <http://doi.org/10.12952/journal.elementa.000091>, 2016b.
- 715 Sun, R. Y., Jiskra, M., Amos, H. M., Zhang, Y. X., Sunderland, E. M., and Sonke, J. E.: Modelling the
716 mercury stable isotope distribution of Earth surface reservoirs: Implications for global Hg
717 cycling, *Geochim Cosmochim Acta*, 246, 156-173, 10.1016/j.gca.2018.11.036, 2019.
- 718 Swartzendruber, P. C., Jaffe, D. A., and Finley, B.: Development and First Results of an Aircraft-Based,
719 High Time Resolution Technique for Gaseous Elemental and Reactive (Oxidized) Gaseous
720 Mercury, *Environmental Science & Technology*, 43, 7484-7489, Doi 10.1021/Es901390t, 2009.
- 721 Tang, S., Feng, C., Feng, X., Zhu, J., Sun, R., Fan, H., Wang, L., Li, R., Mao, T., and Zhou, T.: Stable isotope
722 composition of mercury forms in flue gases from a typical coal-fired power plant, Inner
723 Mongolia, northern China, *J Hazard Mater*, 328, 90-97,
724 <http://dx.doi.org/10.1016/j.jhazmat.2017.01.014>, 2017.
- 725 Tang, Y., Wang, S. X., Wu, Q. R., Liu, K. Y., Wang, L., Li, S., Gao, W., Zhang, L., Zheng, H. T., Li, Z. J., and
726 Hao, J. M.: Recent decrease trend of atmospheric mercury concentrations in East China: the
727 influence of anthropogenic emissions, *Atmos Chem Phys*, 18, 8279-8291, 2018.
- 728 USEPA: Method 1631, Revision E: Mercury in Water by Oxidation, Purge and Trap, and Cold Vapor
729 Atomic Fluorescence Spectrometry, United States Environmental Protection Agency, 10-46,
730 2002.
- 731 Wang, D. Y., He, L., Shi, X. J., Wei, S. Q., and Feng, X. B.: Release flux of mercury from different
732 environmental surfaces in Chongqing, China, *Chemosphere*, 64, 1845-1854, DOI
733 10.1016/j.chemosphere.2006.01.054, 2006.
- 734 Wang, X., Lin, C. J., Yuan, W., Sommar, J., Zhu, W., and Feng, X. B.: Emission-dominated gas exchange
735 of elemental mercury vapor over natural surfaces in China, *Atmos Chem Phys*, 16, 11125-11143,
736 2016.
- 737 Wu, Q. R., Wang, S. X., Li, G. L., Liang, S., Lin, C. J., Wang, Y. F., Cai, S. Y., Liu, K. Y., and Hao, J. M.:
738 Temporal Trend and Spatial Distribution of Speciated Atmospheric Mercury Emissions in China
739 During 1978-2014, *Environmental Science & Technology*, 50, 13428-13435, 2016.
- 740 Xu, H., Sonke, J. E., Guinot, B., Fu, X., Sun, R., Lanzanova, A., Candaudap, F., Shen, Z., and Cao, J.:
741 Seasonal and Annual Variations in Atmospheric Hg and Pb Isotopes in Xi'an, China, *Environ Sci
742 Technol*, 51, 3759-3766, 10.1021/acs.est.6b06145, 2017.
- 743 Yu, B., Fu, X., Yin, R., Zhang, H., Wang, X., Lin, C.-J., Wu, C., Zhang, Y., He, N., Fu, P., Wang, Z., Shang, L.,
744 Sommar, J., Sonke, J. E., Maurice, L., Guinot, B., and Feng, X.: Isotopic Composition of
745 Atmospheric Mercury in China: New Evidence for Sources and Transformation Processes in Air
746 and in Vegetation, *Environmental Science & Technology*, 50, 9262-9269,
747 10.1021/acs.est.6b01782, 2016.
- 748 Zhang, H., Wang, Z. W., Wang, C. J., and Zhang, X. S.: Concentrations and gas-particle partitioning of
749 atmospheric reactive mercury at an urban site in Beijing, China, *Environ Pollut*, 249, 13-23,
750 10.1016/j.envpol.2019.02.064, 2019.
- 751 Zhang, L., Wang, S. X., Wang, L., and Hao, J. M.: Atmospheric mercury concentration and chemical
752 speciation at a rural site in Beijing, China: implications of mercury emission sources, *Atmos
753 Chem Phys*, 13, 10505-10516, DOI 10.5194/acp-13-10505-2013, 2013.



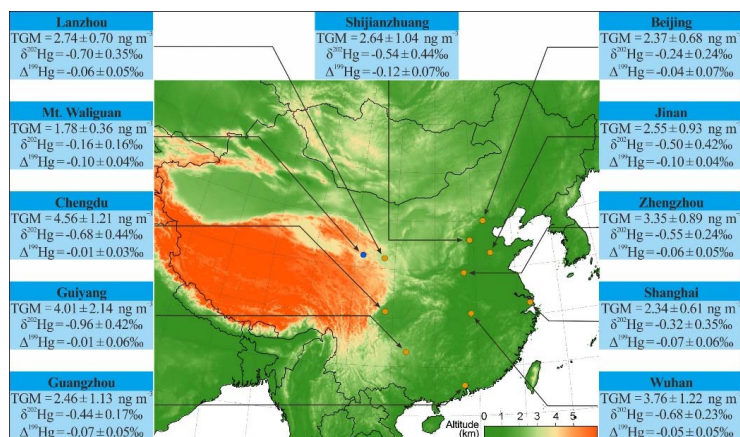
754 Zheng, B., Tong, D., Li, M., Liu, F., Hong, C. P., Geng, G. N., Li, H. Y., Li, X., Peng, L. Q., Qi, J., Yan, L., Zhang,
755 Y. X., Zhao, H. Y., Zheng, Y. X., He, K. B., and Zhang, Q.: Trends in China's anthropogenic
756 emissions since 2010 as the consequence of clean air actions, *Atmos Chem Phys*, 18, 14095-
757 14111, 10.5194/acp-18-14095-2018, 2018.

758 Zheng, W., and Hintelmann, H.: Nuclear Field Shift Effect in Isotope Fractionation of Mercury during
759 Abiotic Reduction in the Absence of Light, *J Phys Chem A*, 114, 4238-4245, 2010.

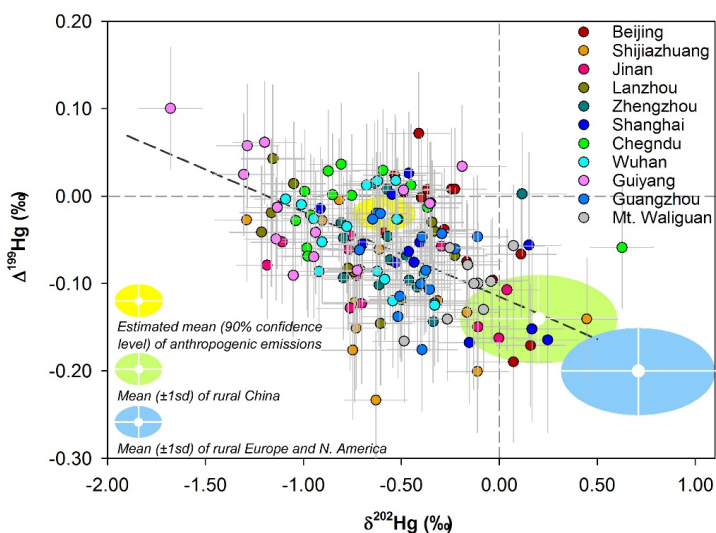
760 Zhu, J., Wang, T., Talbot, R., Mao, H., Hall, C. B., Yang, X., Fu, C., Zhuang, B., Li, S., Han, Y., and Huang,
761 X.: Characteristics of atmospheric Total Gaseous Mercury (TGM) observed in urban Nanjing,
762 China, *Atmos Chem Phys*, 12, 12103-12118, DOI 10.5194/acp-12-12103-2012, 2012.

763

764

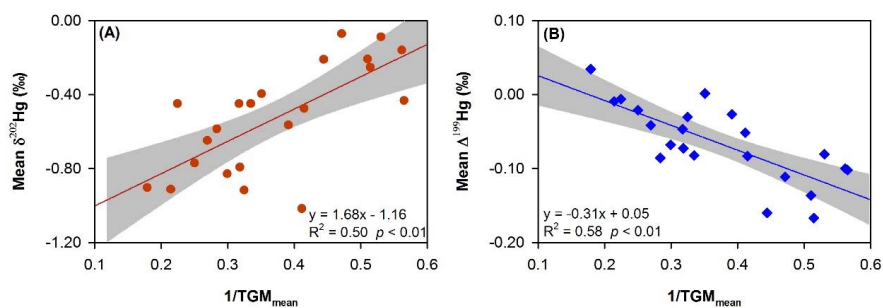


765
 766 Figure 1 TGM mean concentrations ($\pm 1\sigma$), $\delta^{202}\text{Hg}$ ($\pm 1\sigma$) and $\Delta^{199}\text{Hg}$ values ($\pm 1\sigma$) at the ten urban
 767 sites (brown cycle) and one rural site (blue cycle) in China during the whole study periods.
 768
 769



770
771 Figure 2 Mass-dependent ($\delta^{202}\text{Hg}$) and mass-independent ($\Delta^{199}\text{Hg}$) signatures of daily TGM
772 samples collected in the present study (circle) with error bars representing 2σ analytical uncertainty.
773 The shaded areas are the literature-based mean ($\pm 1\sigma$) $\delta^{202}\text{Hg}$ and $\Delta^{199}\text{Hg}$ of TGM or GEM measured
774 in rural areas of China (light green) and Europe and North America (light blue) as well as those
775 estimated for anthropogenic emissions (yellow) (Gratz et al., 2010; Sherman et al., 2010; Demers
776 et al., 2013; Demers et al., 2015; Enrico et al., 2016; Fu et al., 2016; Yu et al., 2016; Obrist et al.,
777 2017; Xu et al., 2017; Fu et al., 2018; Fu et al., 2019; Jiskra et al., 2019a; Jiskra et al., 2019b).
778 Dotted line represents the linear regression between TGM $\delta^{202}\text{Hg}$ and $\Delta^{199}\text{Hg}$ measured in the
779 present study (ANOVA, $R^2 = 0.38$, $p < 0.01$).

780
781



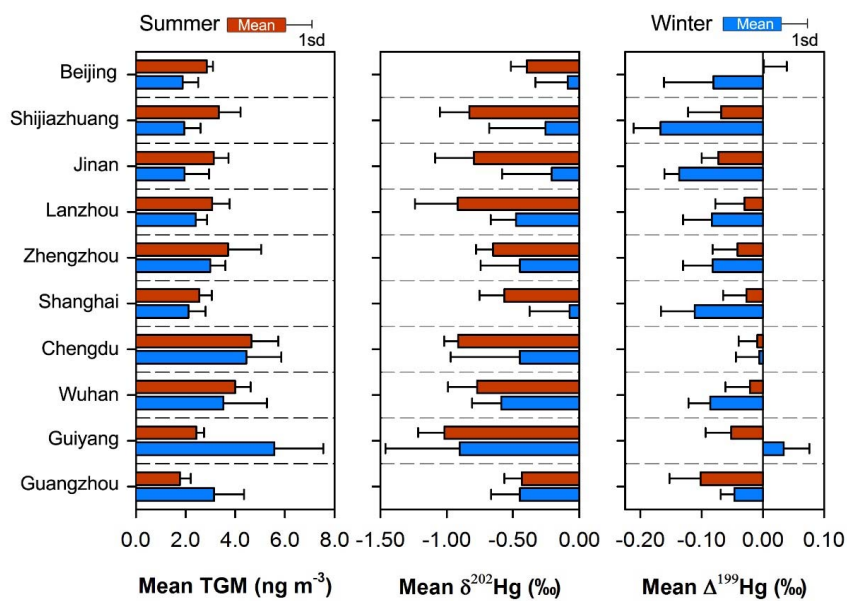
782

783 Figure 3 (A) mean $\delta^{202}\text{Hg}$ versus $1/\text{TGM}$ and (B) mean $\Delta^{199}\text{Hg}$ versus $1/\text{TGM}$ diagrams suggesting
784 a physical binary mixing between the regional-scale background and urbanized source end-member.
785 Lines represent the linear regression of the data and shaded gray area are the 95% confidence area
786 of the regression.

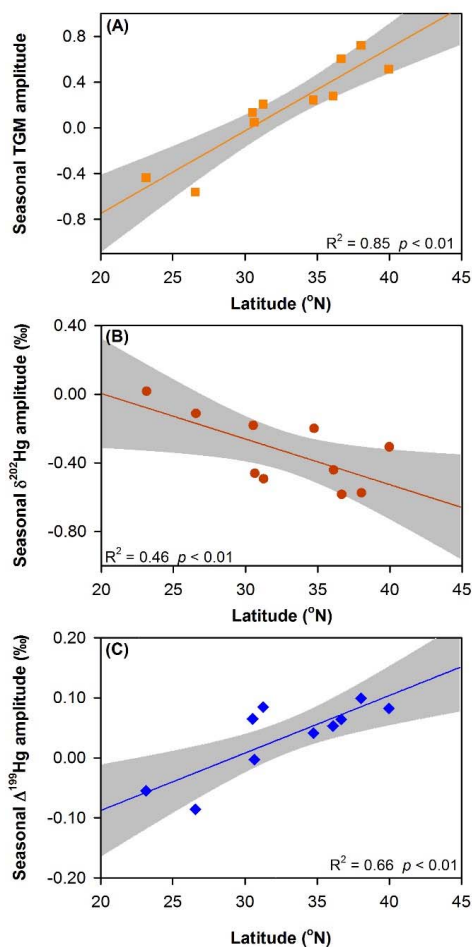
787

788

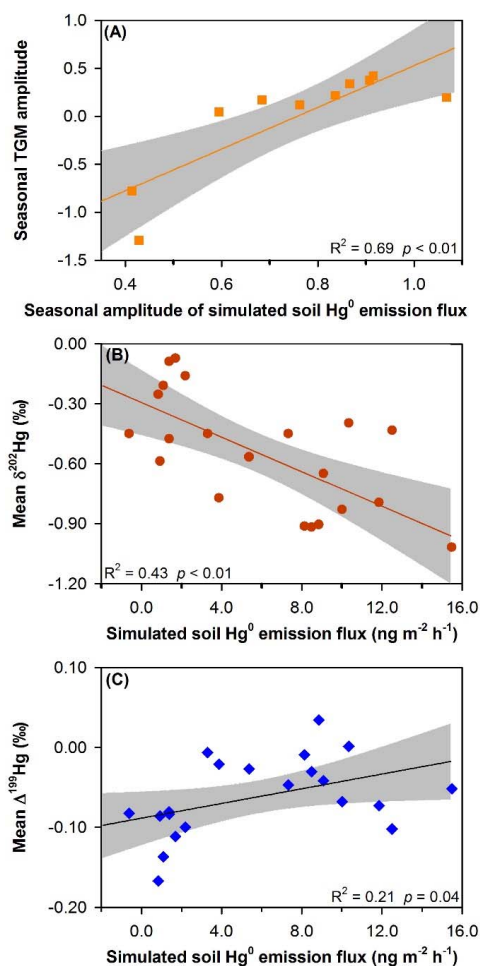
789



790
791 Figure 4 Summertime and wintertime means of TGM concentrations (A), TGM $\delta^{202}\text{Hg}$ (B), and
792 TGM $\Delta^{199}\text{Hg}$ (C) in the ten Chinese cities. Error bars represent 1σ .
793
794



795
796 Figure 5 Latitude dependence of the seasonal variations in TGM concentrations and isotopic
797 compositions in the ten Chinese cities. (A) Seasonal amplitude of TGM concentrations ($(\text{TGM}_{\text{summer}}$
798 $-\text{TGM}_{\text{winter}})/\text{TGM}_{\text{summer}}$) versus latitude. (B) Seasonal amplitude of $\delta^{202}\text{Hg}$ values ($\delta^{202}\text{Hg}_{\text{summer}}$ -
799 $\delta^{202}\text{Hg}_{\text{winter}}$) versus latitude. (C) Seasonal amplitude of $\Delta^{199}\text{Hg}$ values ($\Delta^{199}\text{Hg}_{\text{summer}}$ - $\Delta^{199}\text{Hg}_{\text{winter}}$)
800 versus latitude. Lines represent the linear regression of the data and shaded gray area are the 95%
801 confidence area of the regression.
802



803

804 Figure 6 Effect of soil Hg^0 (GEM) emissions on variations in TGM concentrations and isotopic
805 compositions at the sampling sites in this study. Linear regressions between (A) seasonal TGM
806 amplitude and seasonal amplitude of simulated soil Hg^0 emissions flux, (B) mean TGM $\delta^{202}\text{Hg}$ and
807 simulated soil Hg^0 emissions flux, and (C) mean TGM $\Delta^{199}\text{Hg}$ and simulated soil Hg^0 emissions
808 flux. Lines represent the linear regression of the data and shaded gray area are the 95% confidence
809 area of the regression. Simulated soil Hg^0 emissions fluxes are from Wang et al.(2016).

810

811

812